Multi-Parameter Lamb Wave Tomography

Jae-Seung Choi* and
(Korea Heavy Industries & Construction Co., Ltd.)
Ronald A. Kline
(San Diego State University, USA)

This work shows that it is possible to obtain information about more than one parameter from acoustic field information. A variety of ultrasonic Lamb wave modes were utilized to reconstruct thickness and density of an isotropic plate. An image reconstruction of one parameter (thickness of a plate) was carried out for four cases, i.e., the lowest symmetrical and antisymmetrical modes, and the fastest symmetrical and antisymmetrical Lamb waves among multiple modes. For two parameter reconstructions (thickness and density), the image processing was performed using the lowest symmetrical and antisymmetrical modes simultaneously. In this work, a modified version of algebraic reconstruction technique (ART), which is a form of finite-series expansion method, was employed to reconstruct the ultrasonically computed tomographic images. Results from several sample geometries are presented.

Key Words: Algebraic Reconstruction Technique (ART), Lamb Wave, Tomography, Nondestructive Evaluation (NDE)

1. Introduction

In nondestructive evaluation (NDE), ultrasound has been widely used to detect flaws in a specimen or to measure material properties. Bulk waves known as longitudinal and shear waves, as well as guided waves (e.g. Rayleigh and Lamb waves) are commonly used in nondestructive testing. In recent years, ultrasonic tomography has been spotlighted as one of the most promising new techniques in NDE (Eberhard, 1982).

Computerized tomography (CT) is a nondestructive technique which reconstructs the interior image of structures from externally accessible measurements. Though tomography is principally applied in the medical area with X-rays, it can be used for other types of penetrating radiation and can be used to enhance the imaging capability of other nondestructive testing methods. Specially, the ultrasonic tomographic imaging technique can play an important role in ultrasonic testing to detect flaws and to measure material properties. In this study, we illustrate the use of this approach in the reconstruction of the thickness variation and density distribution of a plate using ultrasonic computerized tomography.

The use of ultrasonic testing to measure thickness of a material from accessible side of a structure is not new. The existing method of pulse-echo C-scan images can show a two-dimensional display, but each measurement shows only the state of a corresponding single testing point. Here, we utilize Lamb waves in conjunction with tomography technique to get the distribution of both thickness and density in a plate. A modified version of the algebraic reconstruction algorithm, which is a kind of finite-series expansion method, is used for Lamb wave tomography.

In conventional reconstruction algorithms, only a single parameter such as velocity, density,

* Corresponding Author,
E-mail : jschoi@hanjung. co. kr
TEL : +82-551-278-3671 ; **FAX** : +82-551-278-8532
Senior Researcher, R&D Center, Korea Heavy Industries & Construction Co., Ltd., 555 Guygok-Dong Changwon Kyungnam, Seoul-Korea Zip Code 641-792. (Manuscript Received November 27, 1998; Revised October 18, 1999)

or amplitude was considered for reconstruction. In many cases, however, it is not enough to get a complete understanding of the material. We commonly need multiple parameters to obtain the full information for a material. For example, two material constant parameters, λ and μ, are needed for complete characterization, even for the analysis of an isotropic material. Therefore, a modified multi-parameter reconstruction technique is applied for the complete analysis of the thickness variation and density distribution of a plate. Kline et al.(1994) demonstrated how the ability to propagate several distinct acoustic wave modes could be exploited tomographically for the reconstruction of the spatial behavior of more than one mechanical property. One practical material characterization problem that has attracted a great deal of interest is the residual stress distribution in a solid media. Choi et al.(1997) have employed multi-parameter acoustic tomography to analyze the residual stress. The study has considered the anisotropy introduced by the presence of residual stress.

Since Rayleigh(1887) first proposed the surface waves which propagate along the free surface of an infinite half-space and Lamb(1917) showed the wave propagation in a plate which has two boundary surfaces, ultrasonic Rayleigh and Lamb waves have been widely used in nondestructive evaluation. However, tomography using these ultrasonic waves is not widely utilized in NDE. Rose et al.(1988) discussed the technique for mapping out interfacial weakness in an adhesive bond structure using plate leaky wave amplitude. Lamb waves along the ray paths were used without the tomographic technique in their work. Jansen et al.(1991a, 1991b, 1992) described the use of tomographic reconstruction techniques to image defects in surfaces using Rayleigh waves and in thin sheets using Lamb waves through the immersion technique. Hutchins et al.(1993) performed ultrasonic Lamb wave experiments in thin aluminum sheets using a pulsed laser source and an electromagnetic acoustic transducer (EMAT) detector. In their work, a form of transform method was used, based on a filtered back-projection algorithm for image processing. Jansen et al. (1994) imaged the damaged region in two polymer composite plate samples using a Lamb wave immersion tomography technique. Nagata et al. (1995) explored a computed tomographic imaging system using laser generation and a dual-probe fiber-optic interferometer detection of Lamb waves. The attenuation of the Lamb waves was measured and used for tomographic reconstruction of the defects in thin aluminum plates. Here, diffraction effects were neglected as straight ray propagation was assumed.

2. Theory

Lamb waves, named after the scientist who first described them in 1917, propagate in a plate with the two boundary surfaces(Lamb, 1917). Here, we consider P and SV waves in a plate where displacements occur both in the direction of wave propagation and perpendicularly to the plane of the plate. A plane harmonic Lamb wave in a plate of thickness $2b$ propagates in the positive x-direction as shown in Fig. 1. Then, we obtain the Rayleigh-Lamb frequency equations for symmetrical and antisymmetrical waves(Kolsky, 1963, Graff, 1991).

$$\frac{\tan sb}{\tan qb}+\left[\frac{4qsk^2}{(k^2-s^2)^2}\right]^{\pm 1}=0 \tag{1}$$

where, $+1$ for symmetrical

-1 for antisymmetrical

$q^2=\frac{\omega^2}{c_L^2}-k^2$ and $s^2=\frac{\omega^2}{c_S^2}-k^2$

k : wave number

c_L : longitudinal wave velocity

c_S : transverse wave velocity

According to the range of the Lamb wave velocity c, the frequency Eq.(1) is altered in the following dimensionless forms.

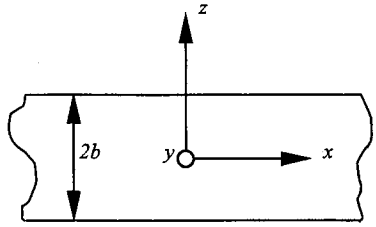

Fig. 1 Coordinate system for a plate

Case I $c<c_S$

$$\frac{\tanh\sqrt{\left(\frac{c_S}{c}\right)^2-1}\,\frac{\omega b}{c_S}}{\tanh\sqrt{\left(\frac{c_S}{c}\right)^2-\left(\frac{c_S}{c_L}\right)^2}\,\frac{\omega b}{c_S}}-\left[\frac{4\left(\frac{c_S}{c}\right)^2\sqrt{\left(\frac{c_S}{c}\right)^2-1}\sqrt{\left(\frac{c_S}{c}\right)^2-\left(\frac{c_S}{c_L}\right)^2}}{\left\{2\left(\frac{c_S}{c}\right)^2-1\right\}^2}\right]^{\pm 1}=0 \tag{2}$$

Case II $c_S<c<c_L$

$$\frac{\tan\sqrt{1-\left(\frac{c_S}{c}\right)^2}\,\frac{\omega b}{c_S}}{\tanh\sqrt{\left(\frac{c_S}{c}\right)^2-\left(\frac{c_S}{c_L}\right)^2}\,\frac{\omega b}{c_S}}\mp\left[\frac{4\left(\frac{c_S}{c}\right)^2\sqrt{1-\left(\frac{c_S}{c}\right)^2}\sqrt{\left(\frac{c_S}{c}\right)^2-\left(\frac{c_S}{c_L}\right)^2}}{\left\{2\left(\frac{c_S}{c}\right)^2-1\right\}^2}\right]^{\pm 1}=0 \tag{3}$$

Case III $c>c_L$

$$\frac{\tan\sqrt{1-\left(\frac{c_S}{c}\right)^2}\,\frac{\omega b}{c_S}}{\tan\sqrt{\left(\frac{c_S}{c_L}\right)^2-\left(\frac{c_S}{c}\right)^2}\,\frac{\omega b}{c_S}}+\left[\frac{4\left(\frac{c_S}{c}\right)^2\sqrt{1-\left(\frac{c_S}{c}\right)^2}\sqrt{\left(\frac{c_S}{c_L}\right)^2-\left(\frac{c_S}{c}\right)^2}}{\left\{2\left(\frac{c_S}{c}\right)^2-1\right\}^2}\right]^{\pm 1}=0 \tag{4}$$

The total number of symmetrical modes N_S that are possible in a plate of given thickness $2b$ at the frequency ω is equal to

$$N_s=1+\left[\frac{2b}{\lambda_S}\right]+\left[\frac{2b}{\lambda_L}+\frac{1}{2}\right] \tag{5}$$

and the total number of antisymmetrical modes, N_a is given as

$$N_a=1+\left[\frac{2b}{\lambda_L}\right]+\left[\frac{2b}{\lambda_S}+\frac{1}{2}\right] \tag{6}$$

The brackets in this case indicate the nearest integer part of the number that they enclose. λ_L and λ_S stand for longitudinal and transverse wavelengths respectively (Viktorov, 1967).

In all of its many forms, tomographic imaging is based on the concept that for radiation propagated through a material, whether electromagnetic or acoustic, the quantities that one can measure experimentally will be line integrals along the path of travel. Generally, we seek to characterize the local nonuniformities in material properties on the basis of measurements of transit time or attenuation. Given the frequency, the Lamb wave velocity depends on the thickness of a plate, as shown in Eq. (1). In this research, the thickness and density in the Lamb wave mode will be used as the main parameters for the tomographic imaging. Other parametric choices are possible.

Before we develop the ART algorithm, a function of n by n variables is defined as

$$f(x_{ij})=f(x_{11},x_{12},x_{13},x_{14},\cdots,x_{nn}) \quad i,j=1,2,3,\cdots,\ n \tag{7}$$

Similarly, we also have

$$f(x_{ij},y_{ij})=f(x_{11},x_{12},x_{13},\cdots,x_{nn},y_{11},y_{12},y_{13},\cdots,y_{nn}) \tag{8}$$

The notations of Eqs. (7) and (8) will be used for convenience here.

In general, parameter X is reconstructed for the image. To reconstruct the tomogaphic images, one begins with a set of initial guesses $(X_{11}^{(0)},X_{12}^{(0)},X_{13}^{(0)},X_{14}^{(0)},\cdots,X_{nn}^{(0)})$ and adjusts these guesses to bring the calculated time delay in line with the measured results. As for conventional ART, one measurement is considered each time. Here, however, the relationship between the time delay and X_{ij} is relatively complicated and does not have a simple form. Therefore, an estimated time delay for the k^{th} iteration is formally written based on the current image profile as

$$T^{(k)}=F(X_{ij}^{(k)}) \tag{9}$$

Then, the current values are updated by adding the modification factors so that the estimated time delay matches the measured time delay. The modification factors are given by

$$\Delta X_{ij}^{(k)}=\lambda_1\frac{\partial F}{\partial X_{ij}^{(k)}} \quad \text{no summation on } i,j \tag{10}$$

where λ_1 is given by the relation

$$\lambda_1=\frac{\Delta T^{(k)}}{\frac{\partial F}{\partial X_{ij}^{(k)}}\frac{\partial F}{\partial X_{ij}^{(k)}}} \quad \text{summation on } i,j \tag{11}$$

Derivations of the modification factors are similar to the processing of two parameters shown later. The partial derivative terms in Eqs. (10) and (11) can be numerically evaluated. In the current study of the Lamb wave tomography, after directly differentiating the time delay with respect to the parameter X_{ij}, i.e., thickness, they are approximated by the numerical method.

Therefore, a typical iteration step for the reconstruction algorithm is given by

$$X_{ij}^{(k+1)}=X_{ij}^{(k)}+\Delta X_{ij}^{(k)} \quad \text{no summation on } i, j \tag{12}$$

For some materials, it is not sufficient to get the full information just by using one-parameter tomographic imaging. In the Lamb wave tomography, the thickness and density of a plate are considered as the reconstruction parameters.

Commonly, we represent the time delays for the lowest symmetrical and antisymmetrical modes in the Lamb waves, as functions of two parameters, X_{ij} and Y_{ij}. Therefore, at each step, we can estimate the time delays for the two modes of waves based on the current values of two parameter profiles (in this study, thickness and density).

$$T_l^{(k)}=F_l(X_{ij}^{(k)}, Y_{ij}^{(k)}) \tag{13}$$
$$T_s^{(k)}=F_s(X_{ij}^{(k)}, Y_{ij}^{(k)}) \tag{14}$$

To match the estimated time delays to the measured time delays, we must add the correction factors to the current values

$$T_l=F_l(X_{ij}^{(k)}+\Delta X_{ij}^{(k)},\ Y_{ij}^{(k)}+\Delta Y_{ij}^{(k)}) \tag{15}$$
$$T_s=F_s(X_{ij}^{(k)}+\Delta X_{ij}^{(k)},\ Y_{ij}^{(k)}+\Delta Y_{ij}^{(k)}) \tag{16}$$

Since the modifications of the images at each step are considered to be small, the above two equations may be linearized using Taylor's series with the nonlinear terms neglected as follows

$$T_l=F_l(X_{ij}^{(k)}, Y_{ij}^{(k)})+\frac{\partial F_l}{\partial X_{ij}^{(k)}}\Delta X_{ij}^{(k)}+\frac{\partial F_l}{\partial Y_{ij}^{(k)}}\Delta Y_{ij}^{(k)} \tag{17}$$

$$T_s=F_s(X_{ij}^{(k)}, Y_{ij}^{(k)})+\frac{\partial F_s}{\partial X_{ij}^{(k)}}\Delta X_{ij}^{(k)}+\frac{\partial F_s}{\partial Y_{ij}^{(k)}}\Delta Y_{ij}^{(k)} \tag{18}$$

where T_l and T_s are the measured time delays.

Using Eqs. (13) and (14), we have from Eqs. (17) and (18)

$$\frac{\partial F_l}{\partial X_{ij}^{(k)}}\Delta X_{ij}^{(k)}+\frac{\partial F_l}{\partial Y_{ij}^{(k)}}\Delta Y_{ij}^{(k)}=\Delta T_l^{(k)} \tag{19}$$

$$\frac{\partial F_s}{\partial X_{ij}^{(k)}}\Delta X_{ij}^{(k)}+\frac{\partial F_s}{\partial Y_{ij}^{(k)}}\Delta Y_{ij}^{(k)}=\Delta T_s^{(k)} \tag{20}$$

where the index summation convention on i, j has been used, and

$$\Delta T_l^{(k)}=T_l-T_l^{(k)} \tag{21}$$
$$\Delta T_s^{(k)}=T_s-T_s^{(k)} \tag{22}$$

For any given acoustic ray and an n by n square array, only Eqs. (19) and (20) are available for $2n^2$ unknowns. It is impossible to solve these equations. This is the same problem that occurs in single parameter reconstruction where a minimum correction criterion is employed to overcome this hurdle and obtain a unique solution. Here we adopt a similar approach. Due to the possibility of different dimensions of the variables, a nondimensional form is desirable. We chose to seek a solution which minimizes the measure of the correction given by

$$\Phi=\frac{\Delta X_{ij}^{(k)}\Delta X_{ij}^{(k)}}{\bar{X}^2}+\frac{\Delta Y_{ij}^{(k)}\Delta Y_{ij}^{(k)}}{\bar{Y}^2} \tag{23}$$

subject to the constraint that the predicted transit times match the measured transit times (Kline et al., 1994, Choi, 1997). Here $\bar{X}$ and $\bar{Y}$ are the average of images over the entire pixels for the two reconstruction parameters. The average values are used for the nondimensionalization because the two parameters generally have different dimensions.

From Eqs. (19) and (20), the constraint equations for the minimum solution problems are

$$\frac{\partial F_l}{\partial X_{ij}^{(k)}}\Delta X_{ij}^{(k)}+\frac{\partial F_l}{\partial Y_{ij}^{(k)}}\Delta Y_{ij}^{(k)}-\Delta T_l^{(k)}=0 \tag{24}$$

$$\frac{\partial F_s}{\partial X_{ij}^{(k)}}\Delta X_{ij}^{(k)}+\frac{\partial F_s}{\partial Y_{ij}^{(k)}}\Delta Y_{ij}^{(k)}-\Delta T_s^{(k)}=0 \tag{25}$$

Then, following the standard Lagrangian multiplier procedure we form the following new function which must be minimized :

$$\begin{aligned}H=&\left(\frac{\Delta X_{ij}^{(k)}\Delta X_{ij}^{(k)}}{\bar{X}^2}+\frac{\Delta Y_{ij}^{(k)}\Delta Y_{ij}^{(k)}}{\bar{Y}^2}\right)\\&+\lambda_1\left(\frac{\partial F_l}{\partial X_{ij}^{(k)}}\Delta X_{ij}^{(k)}+\frac{\partial F_l}{\partial Y_{ij}^{(k)}}\Delta Y_{ij}^{(k)}-\Delta T_l^{(k)}\right)\\&+\lambda_2\left(\frac{\partial F_s}{\partial X_{ij}^{(k)}}\Delta X_{ij}^{(k)}+\frac{\partial F_s}{\partial Y_{ij}^{(k)}}\Delta Y_{ij}^{(k)}-\Delta T_s^{(k)}\right)\end{aligned} \tag{26}$$

Differentiating Eq. (26) with respect to $\Delta X_{ij}^{(k)}$, $\Delta Y_{ij}^{(k)}$, λ_1 and λ_2, to minimize H, we have $2n^2+2$ linear equations with $2n^2+2$ unknowns.

$$\frac{\partial H}{\partial \Delta X_{ij}^{(k)}}=0 \tag{27}$$

$$\frac{\partial H}{\partial \Delta Y_{ij}^{(k)}}=0 \tag{28}$$

$$\frac{\partial H}{\partial \lambda_1}=0 \tag{29}$$

$$\frac{\partial H}{\partial \lambda_2}=0 \tag{30}$$

This yields a solution for the modification factors given by

$$\Delta X_{ij}^{(k)}=-\frac{1}{2}\bar{X}^2\left(\lambda_1\frac{\partial F_l}{\partial X_{ij}^{(k)}}+\lambda_2\frac{\partial F_s}{\partial X_{ij}^{(k)}}\right)$$
no summation on i, j (31)

$$\Delta Y_{ij}^{(k)}=-\frac{1}{2}\bar{Y}^2\left(\lambda_1\frac{\partial F_l}{\partial Y_{ij}^{(k)}}+\lambda_2\frac{\partial F_s}{\partial Y_{ij}^{(k)}}\right)$$
no summation on i, j (32)

where λ_1 and λ_2 are determined by the following equations

$$\left(\bar{X}^2\frac{\partial F_l}{\partial X_{ij}^{(k)}}\frac{\partial F_l}{\partial X_{ij}^{(k)}}+\bar{Y}^2\frac{\partial F_l}{\partial Y_{ij}^{(k)}}\frac{\partial F_l}{\partial Y_{ij}^{(k)}}\right)\lambda_1$$
$$+\left(\bar{X}^2\frac{\partial F_l}{\partial X_{ij}^{(k)}}\frac{\partial F_s}{\partial X_{ij}^{(k)}}+\bar{Y}^2\frac{\partial F_l}{\partial Y_{ij}^{(k)}}\frac{\partial F_s}{\partial Y_{ij}^{(k)}}\right)\lambda_2=-2\Delta T_l^{(k)} \tag{33}$$

$$\left(\bar{X}^2\frac{\partial F_s}{\partial X_{ij}^{(k)}}\frac{\partial F_l}{\partial X_{ij}^{(k)}}+\bar{Y}^2\frac{\partial F_s}{\partial Y_{ij}^{(k)}}\frac{\partial F_l}{\partial Y_{ij}^{(k)}}\right)\lambda_1$$
$$+\left(\bar{X}^2\frac{\partial F_s}{\partial X_{ij}^{(k)}}\frac{\partial F_s}{\partial X_{ij}^{(k)}}+\bar{Y}^2\frac{\partial F_s}{\partial Y_{ij}^{(k)}}\frac{\partial F_s}{\partial Y_{ij}^{(k)}}\right)\lambda_2=-2\Delta T_s^{(k)} \tag{34}$$

Note that the repeated indices summation convention has been applied to i and j.

Therefore, the parameter values for $(k+1)^{th}$ iteration can be expressed as

$$X_{ij}^{(k+1)}=X_{ij}^{(k)}+\Delta X_{ij}^{(k)} \quad \text{no summation on } i, j \tag{35}$$

and

$$Y_{ij}^{(k+1)}=Y_{ij}^{(k)}+\Delta Y_{ij}^{(k)} \quad \text{no summation on } i, j \tag{36}$$

This process is repeated for each ray until convergence is achieved.

3. Results and Discussion

The purpose of nondestructive testing is to measure the dimensions of a material or to investigate the characteristics of the material without damaging or destroying it. In this research, the thickness and density reconstruction of an isotropic plate by the Lamb wave mode was analyzed using the tomographic technique. The transit times were given by the following summation

$$TT_i=\sum_{j=1}^{n^2}D_{ij}m_j \tag{37}$$

Table 1 The properties of aluminum

Lamé's Constants(xE10 Pa)	
λ	μ
5.6	2.6

where TT_i : transit time for i^{th} ray
D_{ij} : distance transversed by i^{th} ray in j^{th} cell
m_j : slowness for the j^{th} cell
(function of reconstruction variables)

The sample was assumed to be aluminum. Table 1 shows the properties of aluminum.

First, we discuss Lamb wave tomography to measure the thickness of a plate. From the one-parameter ART explained in the previous section, an image reconstruction of the synthetic thickness distribution of a plate was obtained for four cases, i.e., the lowest symmetrical and antisymmetrical modes, and the symmetrical and antisymmetrical Lamb wave modes.

Even when Lamb waves propagate in an isotropic plate, analysis is complicated with respect to bulk wave propagation because multiple modes can occur and are usually dispersive. Unlike the bulk waves for which one typically has access to multiple specimen faces, for plate waves the sources and the receivers are both put on the same surface to create the Lamb waves. Here, it was assumed that the Lamb wave velocity can be directly measured in any given direction. A 20×20 pixel reconstruction domain was used for the images of the thickness distribution.

For a given frequency, the number of Lamb waves is finite, depending on the thickness of the plate. Only the lowest Lamb wave modes (symmetrical and antisymmetrical) can be produced for the thin plate. For the lowest symmetrical and antisymmetrical wave tomography, the samples were divided into five horizontal strips having different thicknesses. Thicknesses of 1.8 cm and 1.5 cm were used alternately in the symmetrical case and 1.4 cm and 1.2 cm in the antisymmetrical case. The geometry is shown in Fig. 2. As an arbitrary initial guess, we assumed that the sample rative reconstruction algorithm, choosing either a convergence criterion or the maximum

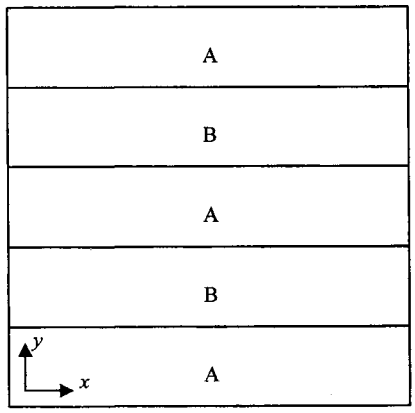

• Symmetry

Region A : thickness=1.8 cm

Region B : thickness=1.5 cm

• Antisymmetry

Region A : thickness=1.4 cm

Region B : thickness=1.2 cm

Fig. 2 Geometry for lowest wave tomography

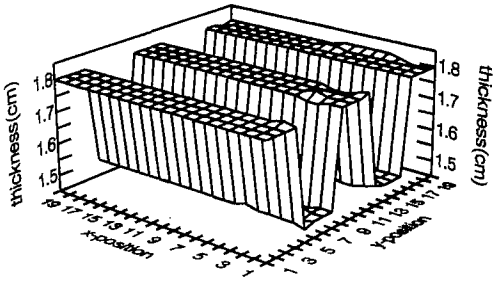

Fig. 3 Thickness tomogram (lowest symmetrical wave)

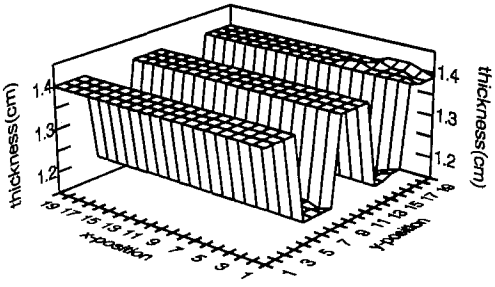

Fig. 4 Thickness tomogram (lowest antisymmetrical wave)

preset number of iterations was required to stop the iteration process. The latter was adopted here

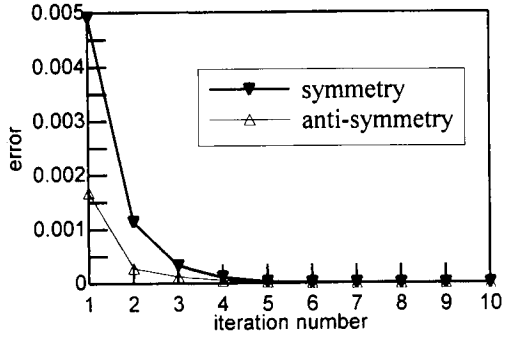

Fig. 5 Convergence behavior (lowest wave mode)

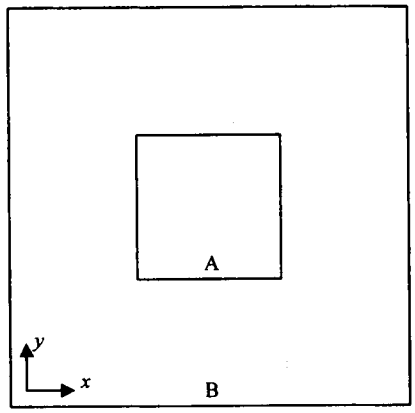

Fig. 6 Geometry for Lamb wave tomography

as most cases showed good reconstructed images after the 10^{th} iteration. Representative results from samples for the lowest symmetrical and antisymmetrical modes are presented in Figs. 3 and 4. The plots consist of a three dimensional representation of the thickness distribution within the sample, with the z-axis representing the computed thickness for each x, y pair (pixel) in the plane of interest. At the 10^{th} iteration, the reconstruction images are similar to the original sample thickness distributions.

The convergence behaviors are shown in Fig. 5. To illustrate the degree of convergence in Fig. 5, for the k^{th} iteration, we have

$$V^{(k)}=\sum_{ij}(b_{ij}^{(k)}-b_{ij}^{(k-1)})^2 \tag{38}$$

where $b_{ij}^{(k)}$ is the thickness in pixel ij.

The lowest wave mode is the particular case of a Lamb wave. Hence, the Lamb wave mode is considered as the general case for thickness image processing. We assumed that the fastest wave

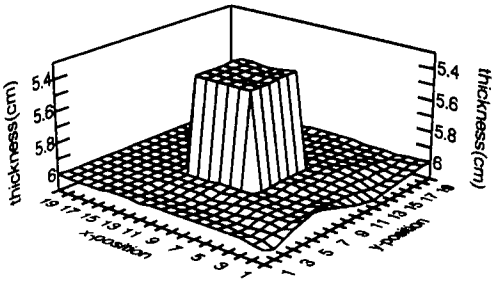

Fig. 7 Thickness tomogram (symmetrical Lamb wave)

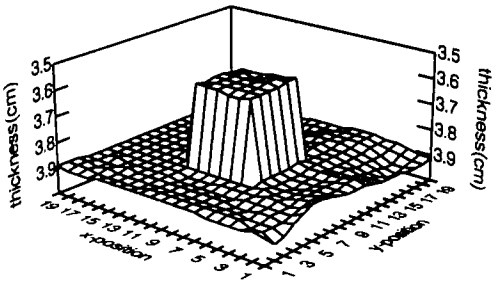

Fig. 8 Thickness tomogram (antisymmetrical Lamb wave)

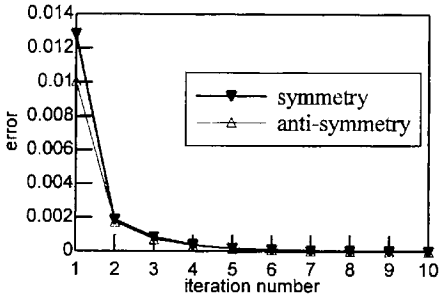

Fig. 9 Convergence behavior (Lamb wave)

among the multiple modes can be measured directly for the given frequency. The reference samples are presented in Fig. 6. The outside part of the sample is thicker than the inside square in both symmetrical and antisymmetrical samples. Figures 7 and 8 show the thickness distribution images for the symmetrical and antisymmetrical Lamb wave cases, respectively, at the 10^{th} iteration. From the reconstructed images, it can be seen that the overall agreement is very good. The convergence behavior is illustrated in Fig. 9.

So far, only one parameter (thickness) has been considered. The next step was to expand the one-parameter Lamb wave tomography to two

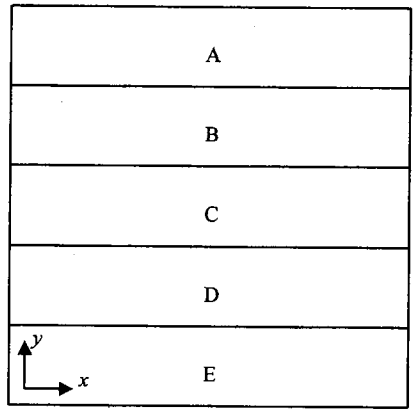

Region	Thickness(cm)	Density(g/cm^3)
A :	1.4	2.7
B :	1.2	2.7
C :	1.4	2.7
D :	1.2	2.6
E :	1.4	2.6

Fig. 10 Geometry for two-parameter Lamb wave tomography

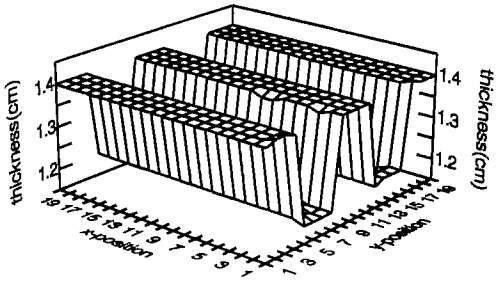

Fig. 11 Two-parameter Lamb wave tomogram (thickness)

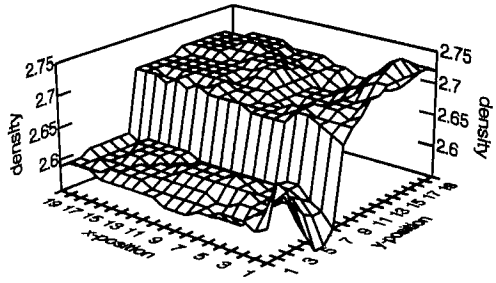

Fig. 12 Two-parameter Lamb wave tomogram (density)

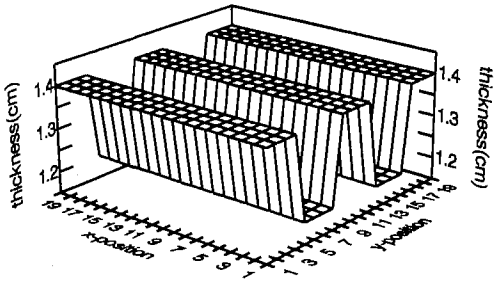

Fig. 13 Two-parameter Lamb wave tomogram in 20th iteration (thickness)

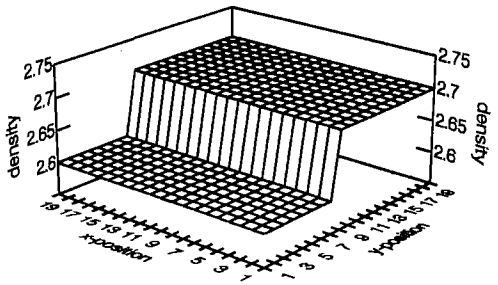

Fig. 14 Two-parameter Lamb wave tomogram in 20th iteration (density)

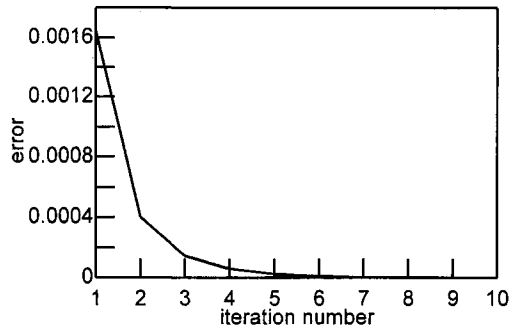

Fig. 15 Convergence behavior (thickness)

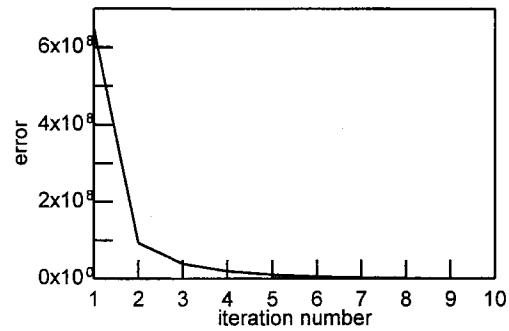

Fig. 16 Convergence behavior (density)

parameters (thickness and density) to obtain a more comprehensive information about the plate since the Lamb wave equation can be expressed as a function of thickness and density. All assumptions were the same as in the previous one-parameter case except that the image processing was performed using the lowest symmetrical and antisymmetrical modes simultaneously. The geometry is illustrated in Fig. 10. Figures. 11 and 12 show the tomographic images for the thickness and the density of the plate at the 10^{th} iteration step. As shown in Figs. 13 and 14, as the iteration number increases, the images approach the original geometry. However, after the 10^{th} iteration, the quality of the images is enhanced only marginally. Figures 15 and 16 present the convergence behaviors for the two parameter reconstructions. Even though the change in reference value is relatively small, it may rapidly converge in 10 iterations with the perfect data acquisition.

Lastly, for the sensitivity analysis, we investigated the effect of synthetic errors on the reconstruction. Potential errors in the measurements may have serious effects on the image processing sought. To examine the reconstruction accuracy, arbitrary potential errors in the measurements were forced into the two parameter reconstructions. To do this, it was assumed that the measured values were distributed in a Gaussian fashion about the actual values. Then, using a norm-statistical routine, each measurement was perturbed according to the normal distribution at a given standard deviation level. The standard error level in the experiment was considered as the standard deviation of its normal distribution. IMSL FORTRAN subroutine codes for statistical analysis were used to generate random numbers from a normal distribution. Under a 0.1% error tolerance there was negligible influence on the reconstructed images. Figures 17 and 18 show the tomogram images at the 0.1% error level. The images are relatively good.

4. Conclusions

Based on the results obtained in this research, the following conclusions can be deduced.

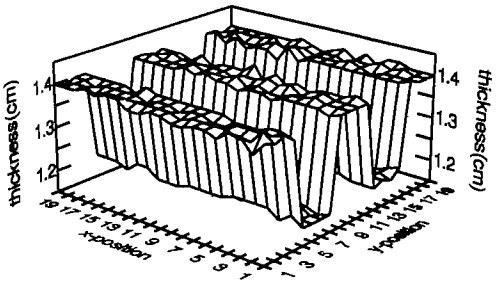

Fig. 17 Two-parameter Lamb wave tomogram at 0.1% error level (thickness)

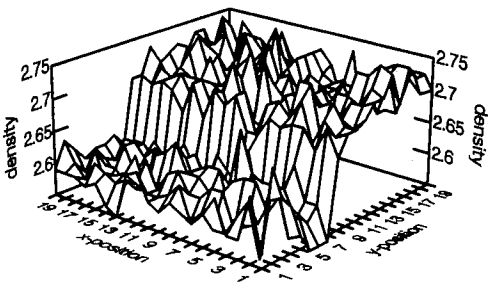

Fig. 18 Two-parameter Lamb wave tomogram at 0.1% error level (density)

Ultrasonic waves were used to investigate the thickness and density distributions of a plate in target materials by computerized tomography (CT). Lamb wave modes were utilized in the thickness and density measurements.

To map out the thickness and density distributions, the modified algebraic reconstruction technique (ART) algorithm, a type of finite-series expansion method, was introduced. For the one parameter reconstruction (thickness), four cases were investigated. For example, the lowest symmetrical and antisymmetrical Lamb wave modes were applied to process the images of thin plates, while for thick plates the fastest symmetrical and antisymmetrical Lamb waves (highest mode) were used. Then, using the lowest symmetrical and antisymmetrical modes simultaneously, the tomographic images for two parameters, the thickness and density of a plate, were reconstructed. Qualitatively and quantitatively, the reconstructed values agreed with the original target values approximately at 10^{th} iteration step in both one- and two-parameter cases.

References

Choi, J. S., and Kline, R. A., 1997, "Residual Stress Analysis Using Multiparameter Tomographic Reconstruction," *Journal of Nondestructive Evaluation*, Vol. 16, No. 3, pp. 121~134.

Eberhard, J. W., 1982, "Ultrasonic Tomography for Nondestructive Evaluation," *Annual Review of Materials Science*, R. A. Huggins, R. H. Bube, and D. A. Vermilyea, eds., Vol. 12, pp. 1~21.

Graff, K. F., 1991, Wave Motion in Elastic Solids, Dover Publications, Inc., New York.

Hutchins, D. A., Jansen, D. P., and Edwards, C., 1993, "Lamb-Wave Tomography Using Non-Contact Transduction," *Ultrasonics*, Vol. 31, No. 2, pp. 97~103.

Jansen, D. P., and Hutchins, D. A., 1991, "Rayleigh Wave Tomography," *Physical Acoustics*, O. Leroy and M. A. Breazeale, eds., pp. 381~384.

Jansen, D. P., and Hutchins, D. A., 1991, "Lamb Wave Tomography," *Proceedings of 1990 IEEE Ultrasonic Symposium* (Hawaii, 1990).

Jansen, D. P., and Hutchins, D. A., 1992, "Immersion Tomography Using Rayleigh and Lamb Waves," *Ultrasonics*, Vol. 30, No. 4, pp. 245~254.

Jansen, D. P., Hutchins, D. A., and Mottram, J. T., 1994, "Lamb Wave Tomography of Advanced Composite Laminates Containing Damage," Ultrasonics, Vol. 32, No. 2, pp. 83~89.

Kline, R. A., Wang, Y. Q., Mignogna, R., and Delsanto, P., 1994, "A New Technique for Multiparameter Image Reconstruction Using a Tomographic Approach," *Review of Progress in Quantitative Nondestructive Evaluation*, Vol. 13, BA.

Kolsky, H., 1963, Stress Waves in Solids, Dover Publications, Inc., New York.

Lamb, H., 1917, "On Waves in an Elastic Plate", *Proc. Roy. Soc.*, London, A93:114~128.

Nagata, Y., Huang, J., Achenbach, J. D., and Krishnaswamy, S., 1995, "Lamb Wave Tomography Using Laser-Based Ultrasonics," *Review of*

Progress in Quantitative Nondestructive Evaluation, D. O. Thompson and D. E. Chimenti, eds., Vol. 14, pp. 561~568.

Rayleigh, J. W. S., 1887, "On Waves Propagated along the Plane Surface of an Elastic Solid," *Proc. London Math. Soc.*, 17:4~11.

Rose, J. L., Nestleroth, J. B., and Balasubramaniam, K., 1988, "Utility of Feature Mapping in Ultrasonic Non-Destructive Evaluation," *Ultrasonics*, Vol. 26, pp. 124~131.

Viktorov, I. A., 1967, *Rayleigh and Lamb Waves, Physical Theory and Applications*, Plenum Press, New York.